Hindawi
Advances in Civil Engineering
Volume 2023, Article ID 6664716, 16 pages
https://doi.org/10.1155/2023/6664716

Research Article

Enhancing Seismic Performance of Steel-Plated Stress-Ribbon Bridge with Tuned Mass Dampers: A Finite-Element Study

Hua Dong[1], **Yi Zhang**[2], **Zhiqiang Huang**[2], **Wuchuan Pu**[3], **Kaiwen Liu**[3] and **Qishuo Zhang**[3]

[1]*China Construction Third Bureau Steel Structure Technology Co., Ltd., Wuhan 430050, China*
[2]*China Construction Third Bureau First Engineering Co., Ltd., Wuhan 430040, China*
[3]*School of Civil Engineering and Architecture, Wuhan University of Technology, Wuhan 430070, China*

Correspondence should be addressed to Wuchuan Pu; puwuchuan@whut.edu.cn

Received 10 June 2023; Revised 25 October 2023; Accepted 8 November 2023; Published 6 December 2023

Academic Editor: Haoran Zuo

There has been a noticeable rise in the construction of lightweight stress-ribbon pedestrian bridges. In regions with a high risk of seismic activity, it is crucial to employ advanced seismic control technology to mitigate the impact of earthquakes and improve the bridge's performance and durability. The objective of this study is to investigate the effect of tuned mass dampers (TMDs) on a steel-plated stress-ribbon bridge using the finite element method. The study aims to analyze the performance of various TMD designs focusing on both vertical and torsional modes. Multiple TMD configurations are considered and numerically compared. The results indicate that TMDs offer both a tuning effect and a static mass effect for stress-ribbon bridges. The tuning effect is most pronounced when the mass ratio falls between 2% and 4%. Installing a single TMD with a mass ratio of 0.05 can decrease vertical displacement along the entire span by up to 36%. Furthermore, a torsional TMD effectively reduces both the torsion of stress ribbons and the pier forces. As a recommendation, the combination of a single vertical displacement TMD and a torsional TMD can be considered the most appropriate scheme for earthquake response control. Moreover, the addition of TMDs reduces the bridge's sensitivity to the direction of earthquake excitation. These findings contribute to a broader understanding of the earthquake performance of stress-ribbon bridges and assist designers in selecting appropriate control schemes to address vibrational issues.

1. Introduction

The stress-ribbon bridge is a prototype of a bridge with a rich history of successful applications. It employs high-strength cables or plates that facilitate vertical load support of the deck slabs, resulting in a need for high horizontal resistance force from the abutment. Given the typically flexible nature of tensioning cables, the bridge has a beautifully curved catenary shape, which enhances its esthetic appeal. As a result, there has been a growing trend toward the construction of the stress-ribbon pedestrian bridge. Recent renowned projects include the Lignon-Loex Bridge in Switzerland, the Slinky Spring to Fame in Germany, and the IGA North Bridge in Germany [1]. While most of the previous stress-ribbon bridges were constructed through a prestressed concrete band, recent advances in high-strength steel materials have prompted the application of steel plates as supporting members of the bridge. These bridges consist of only slender steel bands onto which individual concrete panels are placed, and thus, they are much flexible and lively in their dynamics compared to the prestressed concrete band type.

Stress-ribbon bridges are expected to experience considerable displacement under external dynamic excitations or even asymmetric static loadings. The displacement includes kinetic displacement due to shape changes in the suspension cable and the strain displacement from variations in the material stress, and the former accounts for a large ratio. Some innovative designs of the ribbons have been proposed to advance the applications of new structures and materials. Juozapaitis et al. [2] proposed to use "H" shape section to obtain a bending-stiff ribbon. They demonstrated that a more sustainable deformation behavior of the innovative flexural-stiff ribbons can be achieved compared to the flexible bands of the same axial stiffness. New structural

materials, such as carbon fiber-reinforced polymer, have also been proposed for use in stress-ribbon bridges [3].

On the other hand, the increase of vibration problems of stress-ribbon bridges has been recorded. The estimation, monitoring, and controlling the vibration under dynamic excitations has been a major concern. Moutinho et al. [4] analyzed the vibrational properties of the stress-ribbon footbridge within the University of Porto and proposed to use of an active mass damper to suppress the vibration induced by pedestrians. The AMD was purposely used to overcome the disability of passive TMD tuning to the frequencies of multiple modes; particularly, the structural frequencies themselves may vary with the environmental temperature and operational factors [5–7]. The testing results showed that even with a very small mass ratio (0.15% used in the test), the AMD system can lead to a significant reduction in the acceleration response. Further, Moutinho et al. [8] performed monitoring of the bridge's vibration over several years, with the TMD set to be a passive device and a semiactive device, respectively. It was shown that the passive TMD led to a reduction of vibrations even it was not optimally tuned to any natural frequency, and comparatively, AMD was more effective in attenuating the vibrations. Bleicher et al. [3] proposed to use of a pneumatic muscle actuator to implement active control to the stress-ribbon bridge and conducted a full-scale experiment. The control system can provide sufficient control force while it causes almost no variation in the structural frequency because it is extremely light. Xiao et al. [9] proposed an eddy-current TMD and its parameter optimization method for reducing the excessive vibrations of stress-ribbon bridges under moving vehicle loading.

In view that a single TMD is sensitive to the frequency and multiple modes of a structure maybe triggered, multiple TMD (MTMD) system has been proposed to solve the problem. MTMD has been proposed early by Igusa and Xu [10], where a single TMD was split into several light TMD with frequency ranging around the target value, so that the robustness of the TMD can be improved. The work was intended for solving the single-mode problem, and it has been extensively applied in various scenarios. Another application of multiple TMD is for multimodal control. Multiple TMDs are designed with different vibrational frequencies targeting different modes. Caetano et al. [11] used MTMDs to solve the multimodal vibration problem of a pedestrian bridge in Coimbra, Portugal. Multiple lateral and vertical modes were selected for control. Luo et al. [12] and Chen and Wu [13] successfully allocated MTMDs within structures by using different optimization or search techniques. Daniel et al. [14] investigated the MTMD for multimodal control of pedestrian bridges under pedestrian traffic loading and proposed an iterative analysis/redesign procedure to determine the parameters for a given vibration response limit. Debnath et al. [15] proposed a frequency response function-based strategy, which can be simultaneously applied to multiple modes. Xu et al. [16] proposed a methodology to design a distributed tuned mass damper inerter (TMDI) to obtain the optimized multimode control performance for large-span bridges. In the field of earthquake engineering, Chen and Wu [13] proposed a design strategy of multimode TMD for the control of building structures under earthquake excitation.

Response control technique for stress-ribbon bridge has been mainly focused on the pedestrian and wind loadings [17–21]. However, earthquake is a crucial environmental excitation that stress-ribbon bridges must withstand to ensure structural safety and durability, particularly in areas with higher seismic risk [22]. Although occurring not as frequently as walking or wind loads, earthquakes can cause significantly larger responses than walking or wind-induced responses. Usually, earthquake forces are still the most critical excitation that determines the bridge configuration and member sections. In most cases, stress-ribbon bridges have been designed to withstand static earthquake load. However, this approach is insufficient for designers to fully comprehend the actual dynamic behavior of the bridges during earthquakes. This is especially true for multispan stress-ribbon bridges, which exhibit asymmetric geometries and closely spaced modal frequencies. These characteristics can have a critical impact on the dynamic responses of the bridges [23–28].

TMDs have been widely recognized as one of the most effective methods for controlling structural vibrations [5, 8, 11, 29, 30]. In this study, we aim to evaluate the effectiveness of TMDs in mitigating earthquake-induced vibrations of a stress-ribbon bridge. This specific stress-ribbon bridge stands out due to its utilization of two continuous high-strength steel plates as ribbons, which enhances its vibrational characteristics. To achieve our objectives, a finite element model is developed to analyze the dynamic properties of the bridge. Subsequently, various TMD schemes, including single-mode TMD and multimode TMD, are designed and compared. Section 2 of this study presents the modal characteristics of the stress-ribbon bridge. Section 3 investigates the impact of TMDs on the modal frequencies, demonstrating that the location and mass of the TMDs result in different variations in the modal frequencies. These variations can be attributed to both the static mass effect and the tuning effect. Moving on to Section 4, we present the results of the time history analysis performed on the bridge with different TMD schemes. A comparison is made between the displacements and forces of the bridge with and without TMDs. Moreover, we explore how the responses of the controlled bridges vary when the orientation of the earthquake input is changed.

2. Modal Characteristics of Stress-Ribbon Bridge

2.1. Configuration of the Bridge. This study focuses on the analysis of a two-span pedestrian stress-ribbon bridge. In Figure 1(a), the elevation and geometric dimensions are displayed. Figure 1(b) provides detailed sections of the stress ribbon, while Figure 1(c) illustrates the saddle supporting the stress ribbons. The overall length of the bridge is 88.1 m, with the longer span and shorter span measuring 63.8 and 24.3 m,

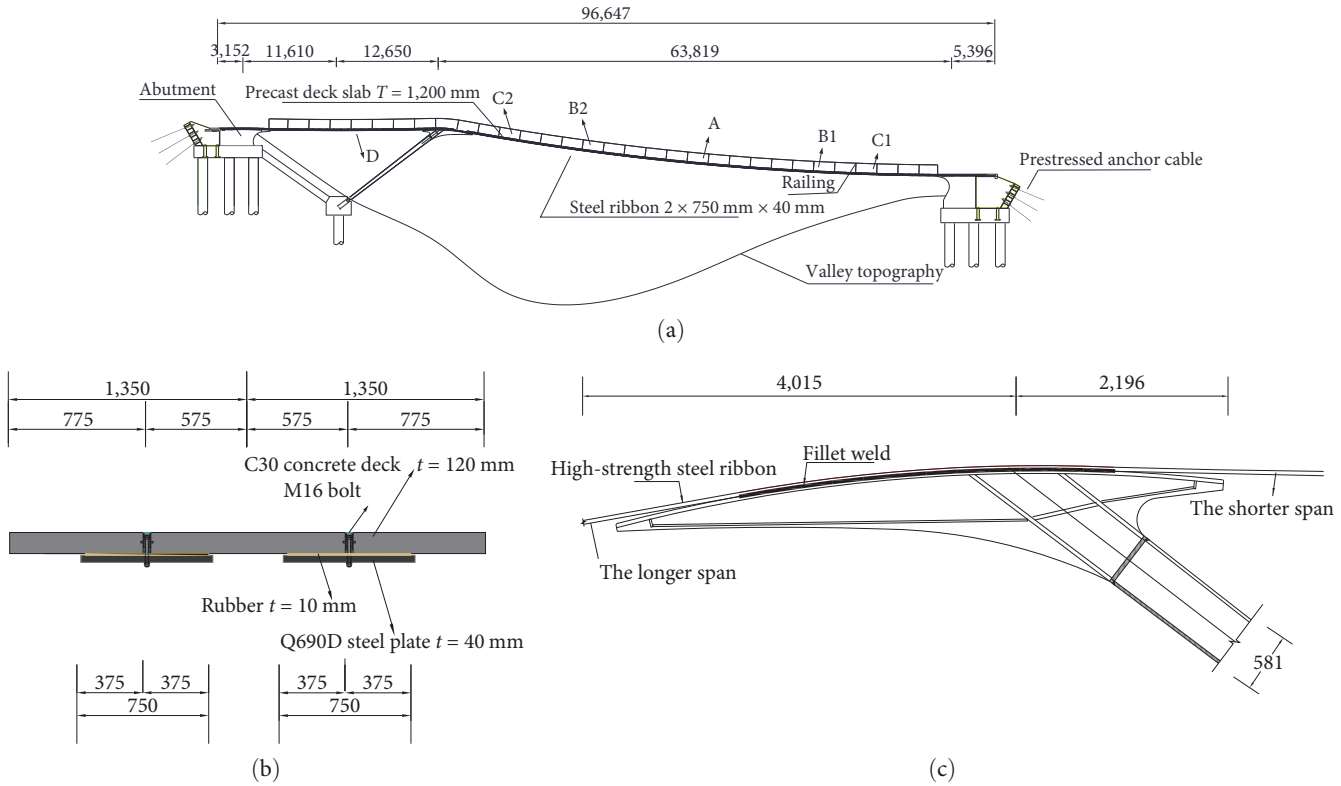

Figure 1: Configuration of the stress-ribbon bridge (unit: mm): (a) the elevation of the bridge; (b) section of the stress ribbon; (c) details of the saddle.

respectively. Under self-weight, the longer span's initial sag is 1.5 m, and the shorter span's initial sag is 0.3 m. The bridge consists of two steel-plate ribbons, with each ribbon 0.75 m wide and 0.04 m thick. The steel plate is made of high-strength steel material (brand Q690D). Previous researches have verified the performance of Q690D steel as a structural material, which can effectively reduce the structural system's weight owing to the high strength [31, 32]. Above the two steel-plated ribbons, the precast concrete deck slabs are installed by using bolts. The bridge is supported by a pier positioned near the high abutment. The pier was constructed at an angle to enhance the bridge's esthetics, and the inclined pier also provides extra tension to balance the axial force's horizontal component at the pier. In the initial stage, the shorter span's horizontal force balances the longer span's horizontal force and the pier's horizontal force component supporting the longer span, as recommended by Strasky's analysis of the bridge's static equilibrium [33].

2.2. Modal Properties of the Bridge. A numerical model of the bridge is established by the finite element program. Figure 2 shows the finite element model and the global coordinate system. In the model, the steel ribbons between the supports are simulated by the beam elements, and the ribbons on the saddle are simulated by the plate element. The beam element is adopted so that the bending stiffness of the ribbon, which is an important influencing factor [34], is taken into account. The saddle on the top of the pier was designed with a curved surface and partially welded with the steel plate. Contact

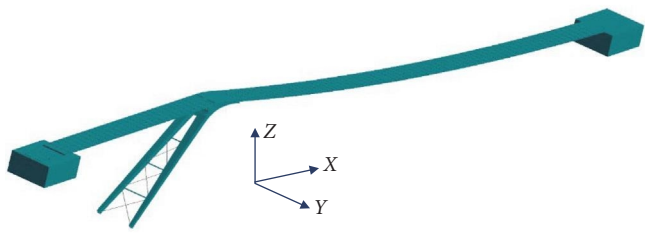

Figure 2: Finite element model of the bridge.

effect exists between the saddle and the steel plate within the nonwielding region. A surface-to-surface contact pair with a friction coefficient of 0.6 is set between the two bodies. The curved saddle was set to be the "target surface" and simulated by the TARGE170 element; the ribbon was set to be the "contact surface" and simulated by the CONTA174 element.

The vertical stiffness of the stress ribbons is greatly influenced by the axial force. A vertical displacement resulting from the vertical loading may cause an increase of the axial force and, thus, the stiffness. It is essential to correctly simulate such a stress-stiffening effect in the numerical model. For stress-ribbon bridge structures made of steel plates, the bending stiffness is small compared to axial stiffness, resulting in a regular nonlinear stiffness matrix produced by large displacement [35, 36]. Such a geometrical nonlinear behavior is modeled by the stress-stiffening function embedded in the

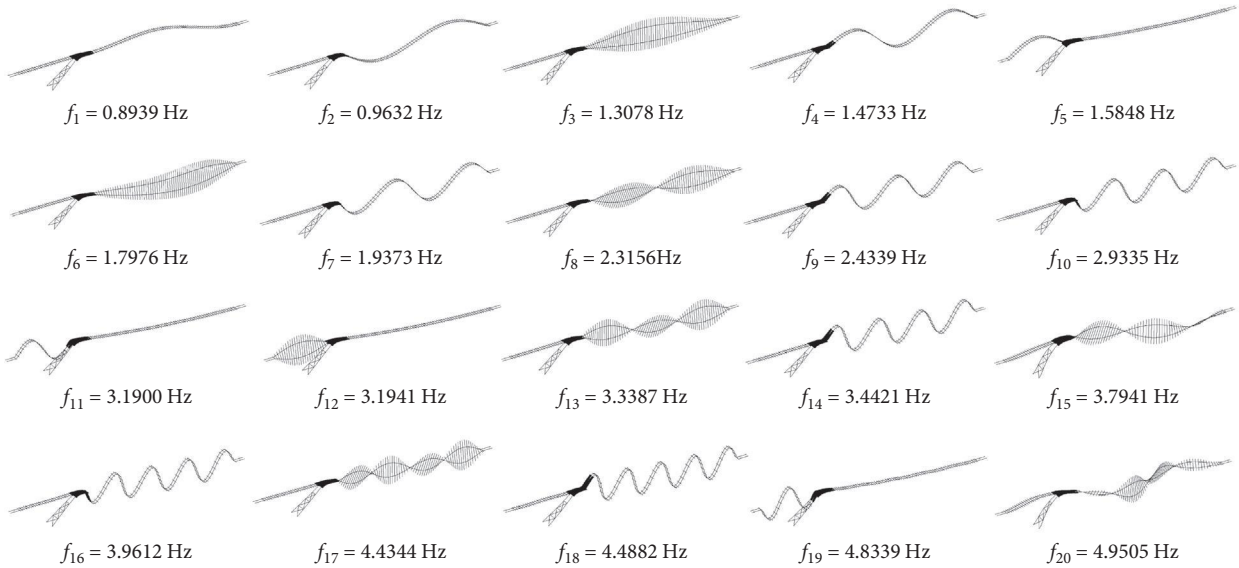

Figure 3: The first 20 vibrational modes of the bridge.

program. The stiffness matrix of geometrical nonlinear structure is represented by a regular material stiffness matrix K_m and an additional stiffness matrix $K_s(\sigma)$, the latter being a function of the stress state. In the program, iteration calculation is carried out to generate the stress stiffness matrix to solve the stress-stiffened problem [37].

Based on the FE model, the modal properties are obtained from the eigenvalue analysis. Figure 3 shows the mode shape and frequencies of the first 20 modes. The frequency ranges between 0.8939 and 4.9505 Hz. Some important vibrational features can be observed. The longer and shorter spans vibrate independently because the obtained vibrational modes are either from the longer or the shorter span. Comparatively, the number of the vibrational modes of the longer span is much more than that of the shorter span. Second, vertical bending is the most frequent pattern of vibration, which includes nine modes of the longer span and three modes of the shorter span. In particular, the first two modes are vertical bending modes resulting from the longer span, which are symmetric and asymmetric modes, respectively. Third, torsion is an essential vibration pattern, and eight modes exhibit apparent torsional motion. The modal frequencies are generally low and close to the neighboring frequencies. The dense modes in the frequency domain suggest that multiple modes may contribute significantly to the responses of the bridge during earthquakes. Based on the vibrational shapes of the first five modes, six locations numbered A, B1, B2, C1, C2, and D, as shown in Figure 1, are defined. Point A is at the center or the two-fold point of the longer span, which experiences the largest amplitude in mode 1 and mode 2. B1 and B2 are the four-fold points of the longer span, and C1 and C2 are the eight-fold points of the longer span, corresponding to the largest amplitude locations of mode 3 and mode 4, respectively. Point D is the center of the shorter span. These locations are considered potential locations for installing TMD.

Previous research has established theoretical formulations for mode frequencies of stress-ribbon bridges. del

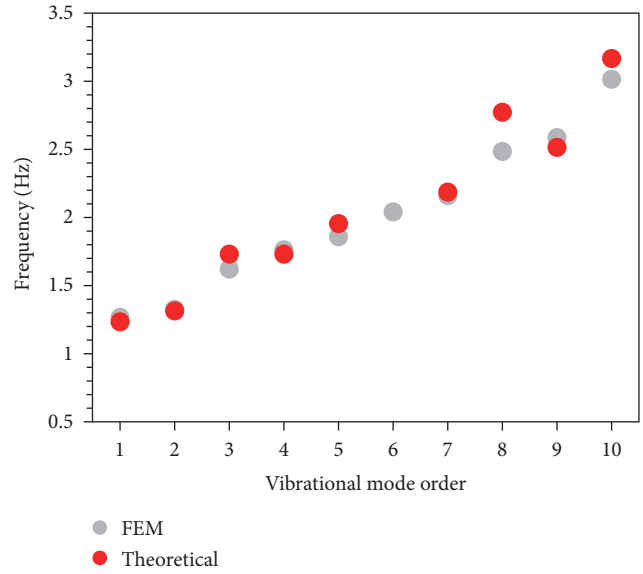

Figure 4: Comparison of the mode frequencies obtained by the FEM model and theoretical methods.

Arco et al. [38] developed a procedure to calculate the frequencies of vertical bending modes with symmetric or asymmetric shapes, assuming the bridge is approximated by pin-supported suspension cable and neglecting bending stiffness. Cacho-Perez et al. [39] derived a technique to obtain the frequency of torsional modes, approximating torsional behavior under clamped–clamped boundary conditions with Saint-Venant torsion theory, which does not incorporate bending or axial effects. Using these procedures, the frequencies of the first ten modes (except for the sixth-order mode) were computed and compared with the FEM-based frequencies in Figure 4. The sixth-order mode is influenced by both torsion and translational vibrations, making its frequency difficult to obtain using existing theoretical formulas for pure bending or

torsion modes. Figure 4 highlights a good agreement between the mode frequencies obtained from the FEM model and the theoretical formulas.

2.3. Transfer Functions of Displacement Responses. To better understand the dynamic responses of the bridge, transfer functions under white noise excitations were derived. A Gaussian white-noise signal was generated using an embedded function in the MATLAB program and inputted in the longitudinal (x), transverse (y), and vertical (z) directions, respectively. The displacement transfer functions were plotted in Figure 5, where the vertical axis $|H(i\omega)|$ represents the complex frequency response function, and the horizontal axis represents the frequency $f(=\omega/2\pi)$. The responses included vertical displacement and torsional angle at point A and vertical displacement at points D, B2, and B1. Comparing the transfer functions obtained from the three input directions, it is evident that the structure responds across a wide frequency range with multiple peaks. For vertical displacement, including points A, D, B2, and B1, the stress-ribbon bridge is more sensitive to z-direction excitation, demonstrated by the large amplitude of the transfer function. However, the torsional response at point A is more sensitive to y-direction excitation. Depending on the location, the response may be excited by multiple vibrational modes, such as vertical displacement at B1 and torsional response at A, as demonstrated by multiple peaks of the transfer function curves in Figures 5(c) and 5(e), respectively. Different locations may be contributed by different vibrational modes since the local peak of the transfer function occurs at multiple frequencies. These results suggest that the control strategy may vary for different control targets of the stress-ribbon bridge.

3. Effect of TMD on Modal Properties

3.1. Determination of the TMD Parameters. Despite the geometric nonlinearity of the stress-ribbon bridge, modal analysis provides crucial references for identifying dominant frequencies. Furthermore, transfer functions show that dynamic actions excite multiple vibrational modes. While TMDs are effective for controlling systems with fixed frequencies, their response control effect is significantly reduced when there is an inconsistency between the frequencies of the main system and the TMD. Therefore, multiple TMDs with different tuned frequencies need to be used to control multiple modes. For each single vibrational mode, TMD parameters can be calculated via the fixed-point theory. The theory establishes two invariant frequency points for a single-degree-of-freedom undamped structure, where the response remains independent of the attached TMD's damping value. According to the fixed-point theory, the optimal frequency ratio $R_{f,\mathrm{opt}}$ and damping ratio ξ_{opt} can be determined by Equations (1) and (2), respectively, where μ represents the mass ratio between the TMD and the main structure [40].

$$R_{f,\mathrm{opt}} = \frac{\sqrt{(1-\mu/2)}}{1+\mu}, \tag{1}$$

$$\xi_{\mathrm{opt}} = \sqrt{\frac{3\mu}{8(1+\mu)(1-\mu/2)}}. \tag{2}$$

The above analysis has shown that both the vertical bending and torsional modes are potential modes that significantly contribute to the responses. Aiming at a vertical bending mode, for a given modal mass ratio μ_b, the required stiffness k_b of the TMD can be calculated by Equation (3), and the damping coefficient c_b is calculated by Equation (4).

$$k_b = m_{tb}{\omega_{tb}}^2 = \frac{\mu_b {M_{sb}}{\omega_{sb}}^2(1-\mu_b/2)}{(1+\mu_b)^2}, \tag{3}$$

$$c_b = 2m_{tb}\omega_{tb}\xi_{opt} = \frac{2\mu_b M_{sb}\omega_{sb}}{1+\mu_b}\sqrt{\frac{3\mu_b}{8(1+\mu_b)}}, \tag{4}$$

where k_b, m_{tb}, ω_{tb}, and c_b denote the stiffness, mass, frequency, and damping coefficient of the TMD for a vertical bending mode, and M_{sb} and ω_{sb} denote the general mass and frequency of a vertical bending mode. In case the torsional mode is controlled, let μ_T denote the ratio of the moment of inertia between the TMD and the structure, and it can be represented by Equation (5).

$$\mu_t = \frac{J_{tt}}{J_{st}} = \frac{2m_{tt}r^2}{J_{st}}, \tag{5}$$

where J_{tt} and J_{st} denote the moment of inertia of TMD and structure, respectively, and m_{tt} and r denote the mass of TMD and the tuning radius of TMD. Similarly, according to Equations (1) and (2), the required stiffness k_t and damping coefficient c_t of the torsional TMD can be calculated by Equations (6) and (7).

$$k_t = \frac{\mu_t m_{tt}{\omega_{st}}^2(1-\mu_t/2)}{(1+\mu_t)^2}, \tag{6}$$

$$c_t = \frac{2\mu_t m_{tt}\omega_{st}}{1+\mu_t}\sqrt{\frac{3\mu_t}{8(1+\mu_t)}}, \tag{7}$$

where ω_{st} is the circular frequency of the structural torsional mode.

3.2. TMD Arrangement Schemes. Since the added mass causes variations in the natural frequencies and a significant mass can alter the bridge's initial shape; therefore, it is recommended to design a TMD with a limited mass. Additionally, the bridge exhibits multiple lower-order modes with closely spaced frequencies, which necessitates further investigation into the distribution of mass for different modes and locations. To meet this requirement, multiple TMD schemes are proposed for numerical comparison. In all of the schemes, an equal mass of TMDs for vertical modes is considered to evaluate the performance of different schemes. The TMD is placed at the location with the highest vibrational amplitude

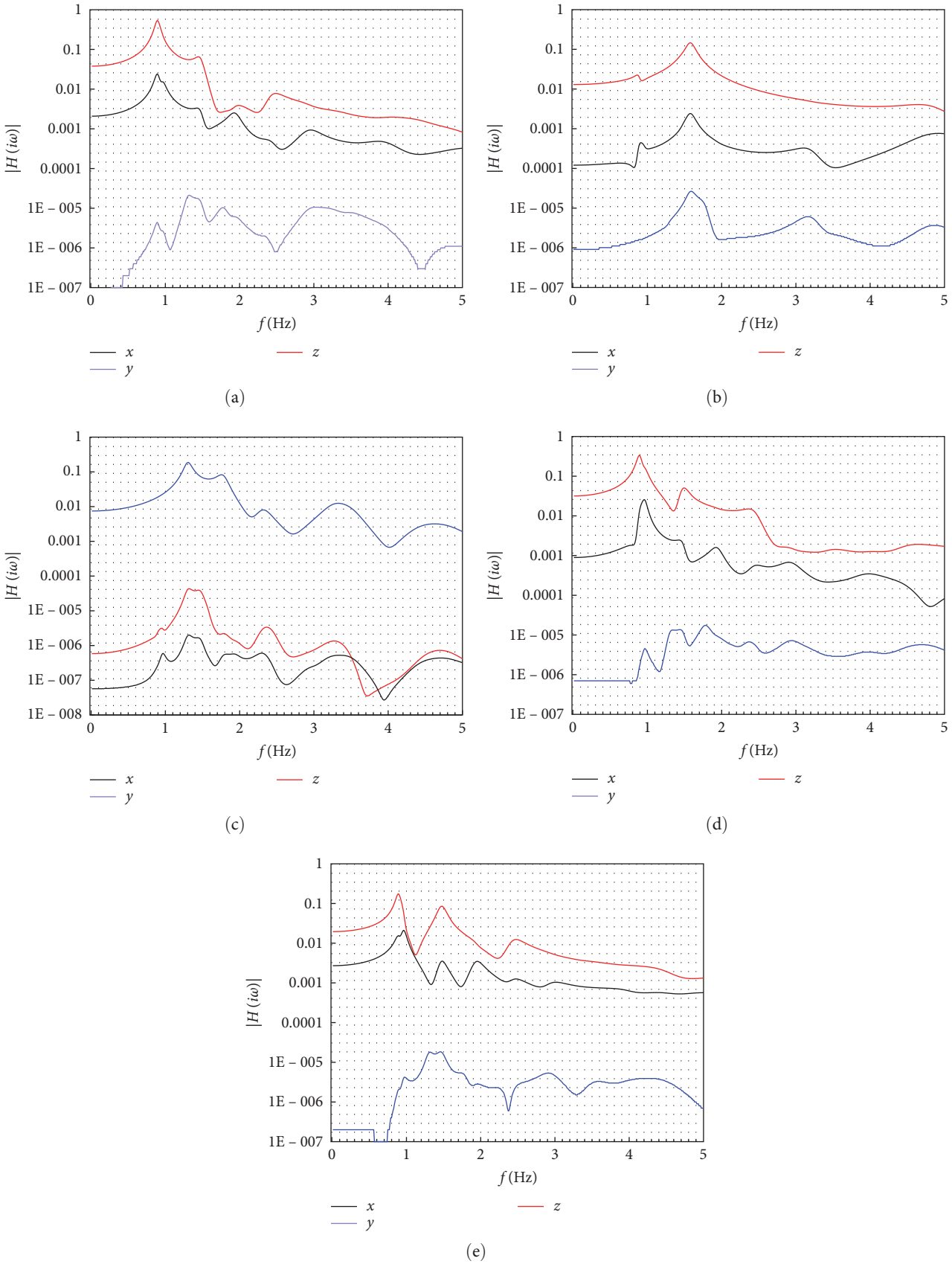

Figure 5: Transfer functions for displacement under different input directions: (a) A: vertical displacement; (b) D: vertical displacement; (c) A: torsional angle; (d) B2: vertical displacement; (e) B1: vertical displacement.

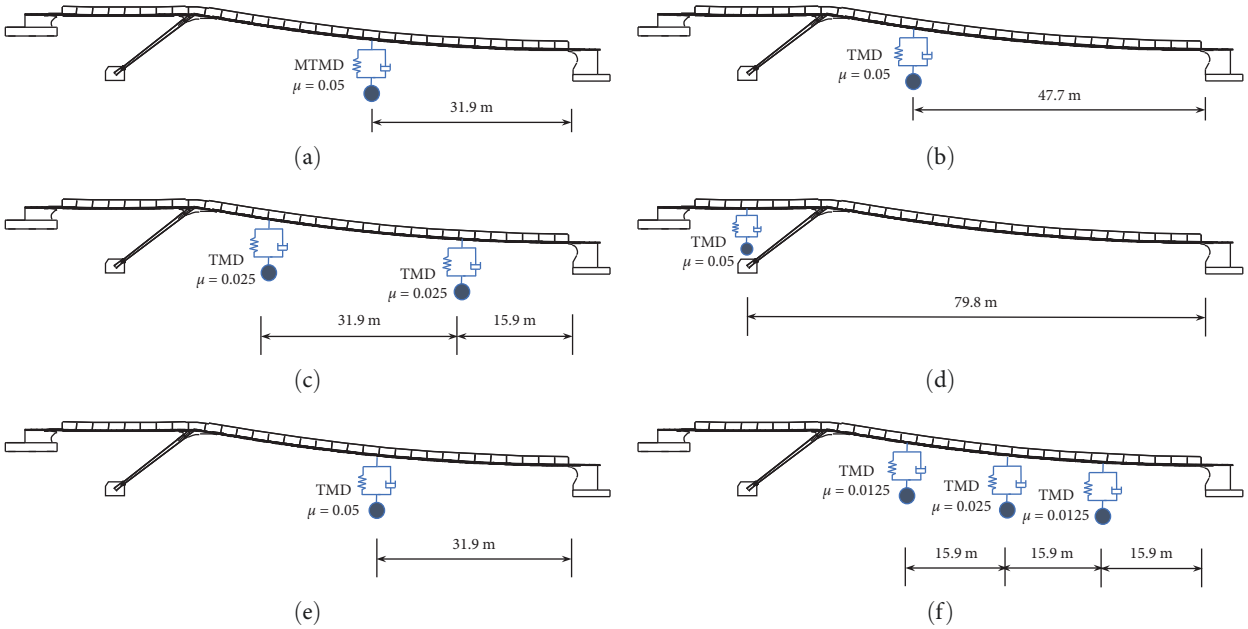

Figure 6: TMD arrangement schemes: (a) no. 1 scheme; (b) no. 2 scheme; (c) no. 3 scheme; (d) no. 4 scheme; (e) no. 5 scheme; (f) no. 6 scheme.

for the targeted mode. Specifically, for mode 1 and mode 3, point A is preferred, while for mode 2, points B1 and B2 are preferred. Figure 6 illustrates the six schemes, with the TMDs arranged as follows:

(1) Scheme no. 1: multimodal TMDs are designed for mode 1 and mode 3. The mass ratio and moment of inertia ratio are both set to 0.05. All TMDs are placed at point A. The torsional TMD consists of a pair of small TMDs, each with a mass equal to 0.39 t, symmetrically suspended on both sides of the section.

(2) Scheme no. 2: a single vertical TMD with a concentrated mass targeted for mode 2 is placed at point B2.

(3) Scheme no. 3: a single vertical TMD with equally distributed mass targeted for mode 2 is placed at points B1 and B2. The scheme allows for a comparison with scheme 2 to understand how the mass distribution affects the performance.

(4) Scheme no. 4: a single vertical TMD with a concentrated mass targeted for mode 5 is placed at point D. While the other schemes focus on the mode of the longer span, this scheme is proposed to evaluate the performance of a TMD placed at the shorter span.

(5) Scheme no. 5: a single vertical TMD with concentrated mass targeted for mode 1 is placed at point A.

(6) Scheme no. 6: multimodal TMDs are used with a distributed mass proportion of 1 : 2 : 1 for points B1, A, and B2, respectively. The scheme is designed to target mode 1 and mode 2.

The stiffness and damping coefficients of each scheme are determined in accordance with the target modes. All the schemes, except scheme 1, have TMDs with the same mass. These schemes were designed to compare the efficiency of concentrated TMD versus distributed TMDs along the bridge.

3.3. Effect of TMD on Modal Frequency. Due to the geometric nonlinearity of the stress ribbon bridge, TMD can produce two control effects: the first is the tuning effect that generating control force that is counter phase to the velocity of the main structure, and the second is the increase in the steel-band stiffness due to additional static mass, which also possibly leads to the variation in dynamic characteristics and displacement reduction of the structural system. To distinguish between these two effects, two working conditions were simulated: TMD locked (infinite stiffness) and TMD unlocked. When the TMD is locked, only the static mass of the TMD is effective, without any tuning control effect. When the TMD is unlocked, it works as a general TMD device; both additional mass effect and tuning effect are active. In order to investigate the influence, modal analysis was conducted on the bridge structure with TMD designed for vertical bending and torsion modes in both working and locked states.

Figure 7 shows the variation of the modal frequencies of the first four modes with a TMD targeting bending or torsion at point A, and the TMD in the working state and locked state are, respectively, considered. The ratios between the modal frequency with TMD and the modal frequency without TMD are presented. Figures 7(a) and 7(b) present the frequencies obtained from a TMD-targeted mode 1. When the TMD is locked, the static mass effect caused a decrease in the frequency of mode 1 from 0.89 to 0.79 Hz, with the mass ratio increased from 0 to 0.1, represented by the ratio decreased from 1 to 0.88. If the TMD is unlocked, the decrease in the frequency of mode 1 is more significant, and the frequency ratio reaches 0.73 for a mass ratio equal to 0.1. Mode 2 and mode 4 are also influenced by the TMD by different degrees; however, mode 3 is almost not affected.

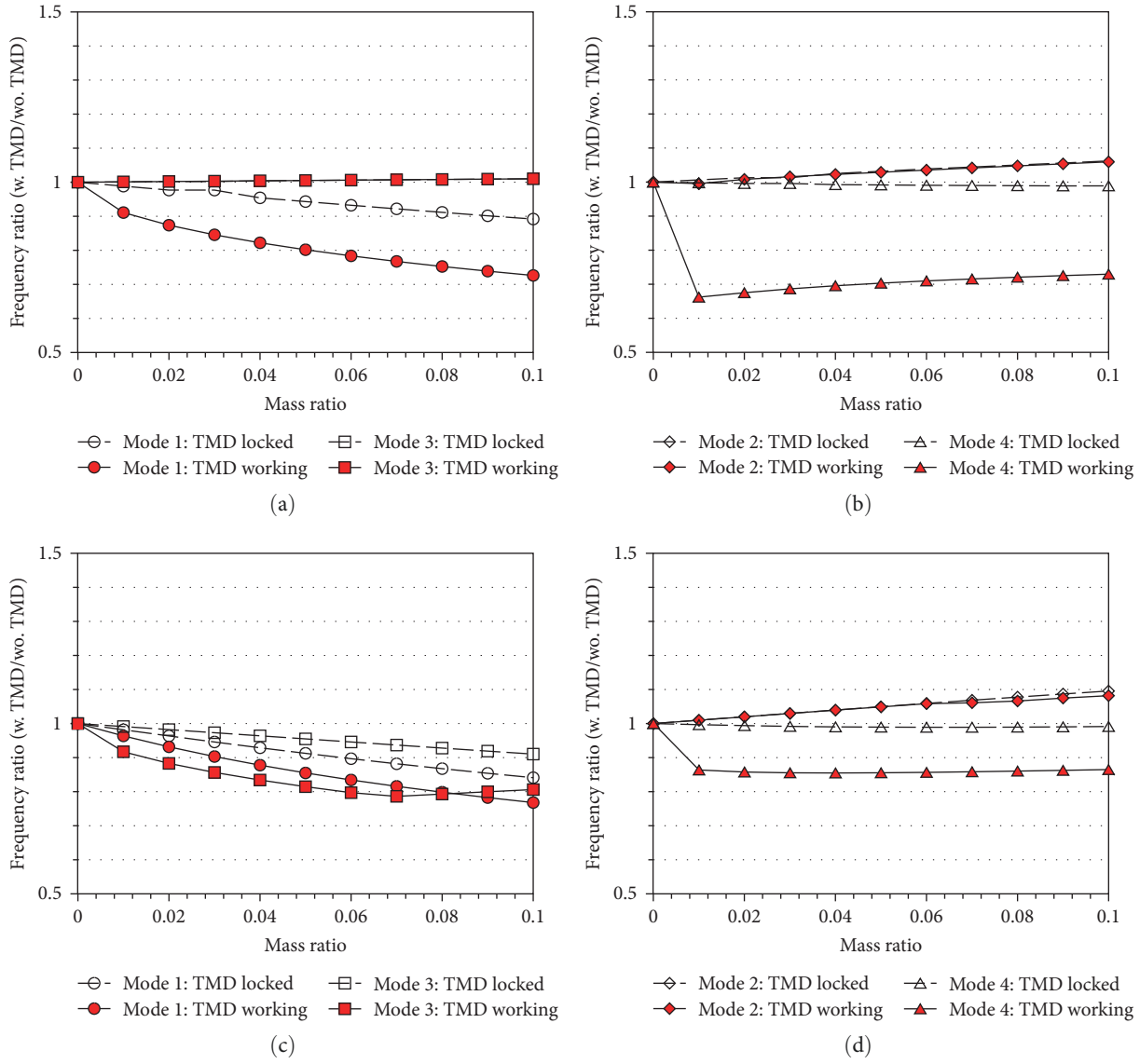

Figure 7: The modal frequency ratio (with damper/without damper) varied with mass ratio and rotational inertia ratio: (a) vertical TMD-induced variation in mode 1 and mode 3; (b) vertical TMD-induced variation in mode 2 and mode 4; (c) rotational TMD-induced variation in mode 1 and mode 3; (d) rotational TMD-induced variation in mode 2 and mode 4.

Figures 7(c) and 7(d) present the frequency variation resulting from the TMD-targeted mode 3. The frequency ratio of mode 3 decreased to 0.91 and 0.81 for TMD locked and TMD unlocked states, respectively. At the same time, the frequencies of other bending modes are also changed due to the static mass effect. Mode 1 and mode 4 are symmetric modes; their frequencies are decreased due to the added TMD. Mode 2 is an asymmetric mode; adding TMD at the center provides additional constraints to the center and thus leads to an increase in its frequency.

The analysis indicates that the addition of TMD to the flexible stress-ribbon bridge results in significant variation in modal frequencies. The sensitivity of frequency to TMD depends on factors such as the location of TMD, modal shape, and mass ratio or moment of inertia ratio. This variation arises due to the tuning effect and the static mass effect of the TMD. Hence, designers should consider such effects when searching for optimal parameters during TMD design.

4. Earthquake Response of Stress-Ribbon Bridge with TMDs

4.1. Tuning Effect of TMD in Earthquake Response. The previous section analyzed the impact of additional TMD on the vibrational frequencies. To investigate the control effect of the TMD system under seismic excitation, a TMD was added at point A to control vertical displacement and different mass ratios were analyzed. The damping and stiffness of the corresponding TMD were calculated according to the fixed-point theory, with the effect of TMD on the vibrational frequency was considered. The stiffness and damping of TMD were simulated using the Combin14 unit, and the

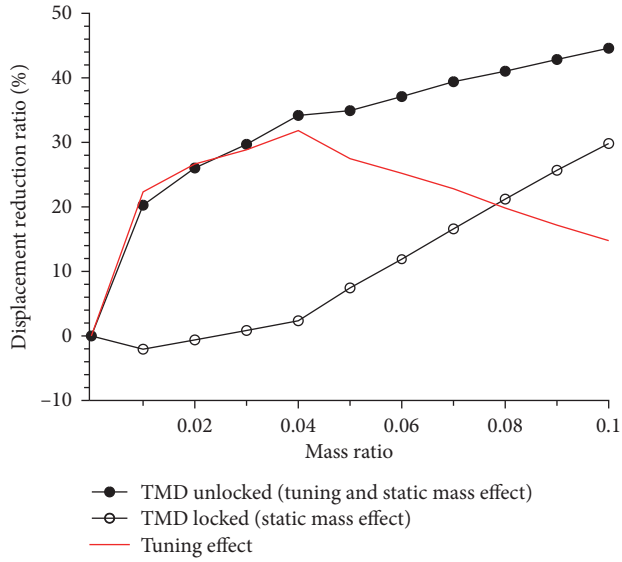

Figure 8: Separation of tuning effect and static mass effect.

mass was simulated using the Mass21 unit. In the numerical model, the inherent damping is simulated by Rayleigh damping, and the damping ratios of the first two modes are set to 0.02. Soria et al. [7] conducted an identification of the damping ratio of a stress-ribbon bridge based on its operational conditions and found it to be approximately 1%. Since larger amplitudes can potentially be excited during earthquakes, resulting in an increase in the damping ratio, a value of 0.02 is assumed in the current study. The RSN978 record from the PEER [41] strong ground motion database was selected as the seismic excitation, with a peak acceleration of 0.25 g.

Figure 8 compares the displacement reduction ratio of point A varying with mass ratio. The tuning effect of the TMD was calculated by subtracting the damping reduction rate of the TMD locked from that of the TMD unlocked. It is observed that when the mass ratio is less than 2%, the additional mass did not cause the dynamic displacement to decrease but rather caused a slight increase. When the mass ratio exceeds 3%, the additional mass generates a controlling effect on the dynamic displacement, and the response reduction ratio increases with the mass ratio.

The tuning effect of the TMD was obtained by dividing the reduction ratio of unlocked TMD by that of locked TMD. The tuning effect increased first and then decreased with the mass ratio, with the optimal tuning effect reaching 31.83% when the mass ratio was 0.04. These results confirm that TMD for stress-ribbon bridges will produce two effects: static mass and dynamic tuning effect. Static mass changes the stiffness of the bridge, and depending on the relative proportion of increased mass and stiffness, the added static mass may cause either a positive or negative control effect. A very small static mass may cause an increase in displacement, while a large mass can decrease the displacement. On the other hand, the tuning effect can produce a good control effect even under a small mass ratio. When the mass ratio is between 2% and 4%, the tuning effect reaches the best. The previous research has shown that a greater mass ratio of TMD leads to a better control effect. However, the benefit of increasing mass becomes insignificant as the mass becomes large. Considering the influence of installation and cost, a mass ratio between 2% and 5% is commonly recommended for large structures. For the stress-ribbon bridge, increasing the mass of TMD always leads to a better control effect on the dynamic displacement. However, it does not mean that increasing the mass necessarily leads to an improved tuning effect. Thus, selecting an appropriate mass ratio is important. Based on the results of Figure 8, a mass ratio of 2%–4% is preferred.

4.2. Comparison of Control Effects of Different TMD Schemes. Time history analysis was performed on the bridge with and without TMDs. Four earthquake records with the record sequence number (RSN) of 956, 978, 1004, and 6889 were downloaded from the PEER strong motion database [41] and used in the analysis. For the two horizontal components of each record, the peak acceleration of the stronger component is scaled to 0.4 g, and the other horizontal component and the vertical component were then scaled with the same proportion. The horizontal component with a large PGA was inputted in the Y-direction of the bridge, while the other was for the X-direction. The maximum vertical displacement of points A, B1, B2, and D and the maximum torsional angle of point A were determined from the dynamic response histories. The vertical accelerations and displacements at points A, B1, B2, and D resulted from scheme 1 are compared with the responses without TMD, as shown in Figure 9. Adding TMD significantly reduces both the displacement and acceleration. On average, the maximum displacement at point A was reduced by 40%, and the root mean square of the time history was reduced by 46%; correspondingly, the maximum and the root mean square of the vertical acceleration were reduced by 46% and 43%, respectively. It is also of interest to compare the responses at points B1, B2, and D. The current TMD design leads to a reduction in vertical displacement and acceleration at B1 by an average of 21% and 18%; B2 by 15% and 21%, and D by 11% and −1%, respectively. Obviously, the TMD brings a control effect for B1 and B2, and even the displacement at D, but caused a light increase in the acceleration at D.

Figure 10 shows the control ratios for all the schemes, where the horizontal axis denotes the scheme number. The responses include the torsional angle at point A and the vertical displacements at points A, D, B1, and B2. The blue bar indicates that the response is reduced after adding TMD, while the red one indicates the response is amplified. The first column shows the torsional response at point A, which demonstrates that the torsion can only be effectively reduced by a torsional TMD (scheme no.1), and a moment of inertia ratio of 0.05 leads to a reduction in the torsion response by about 25%.

Scheme no. 4, which incorporates a single TMD located at point D, demonstrates no noteworthy impact on the response of the longer span. Conversely, all the other schemes that position the TMD at the longer span exhibit

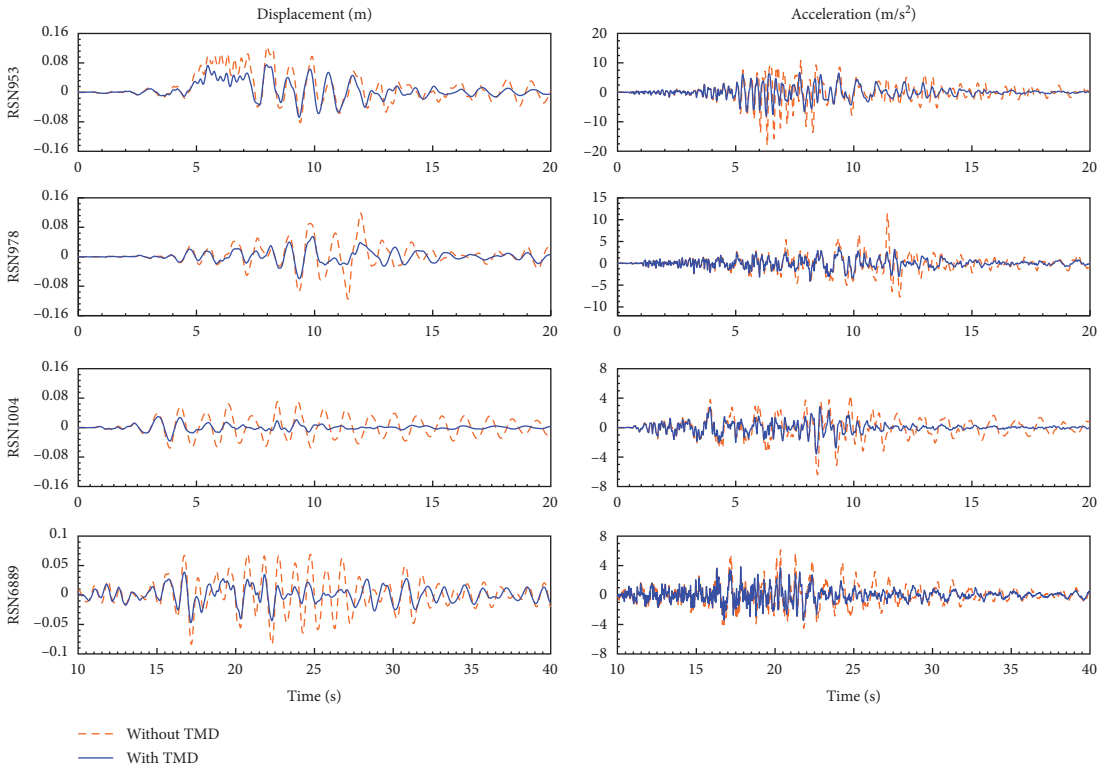

(a)

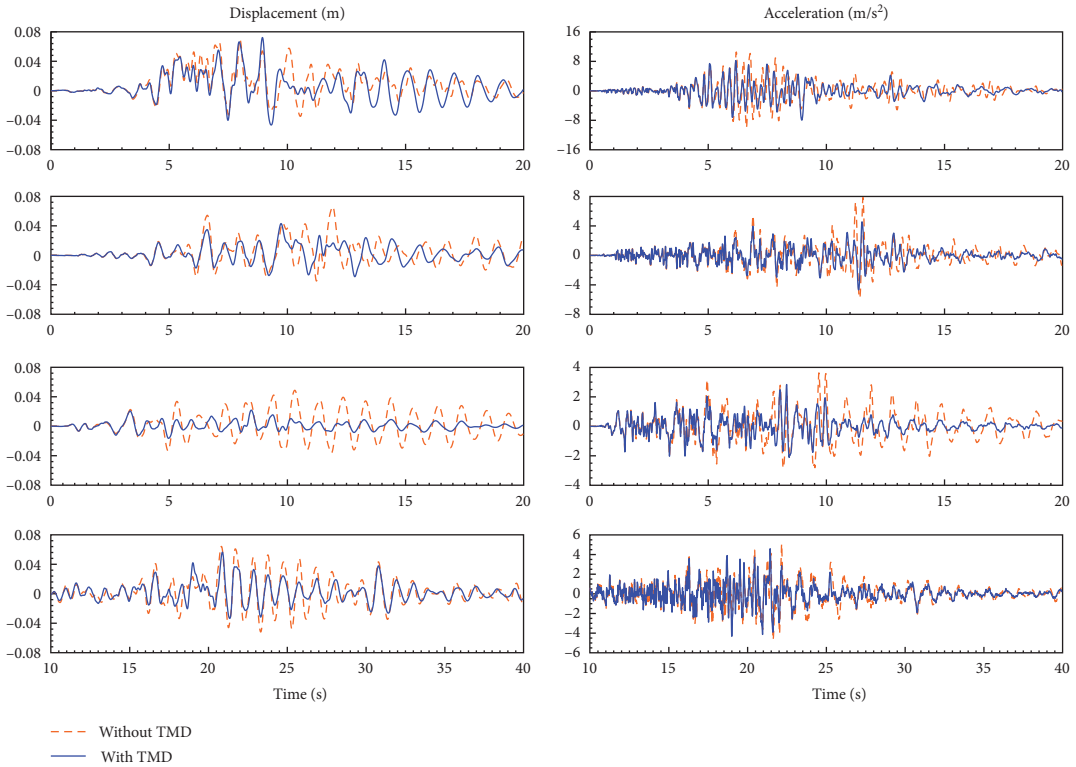

(b)

Figure 9: Continued.

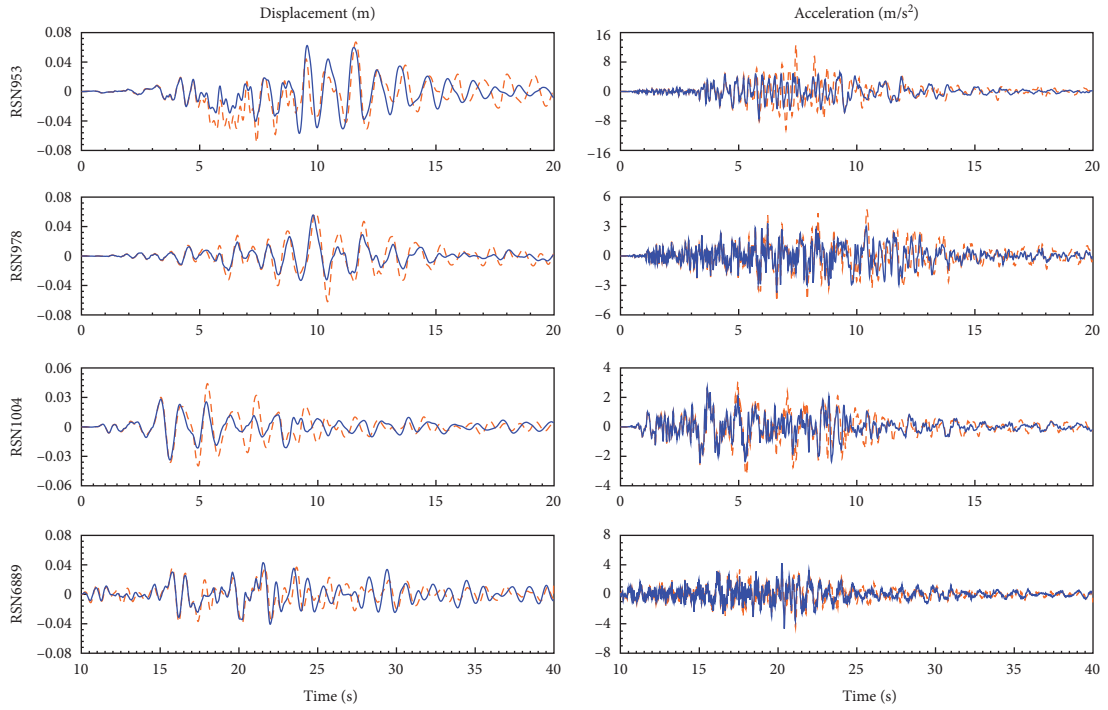

(c)

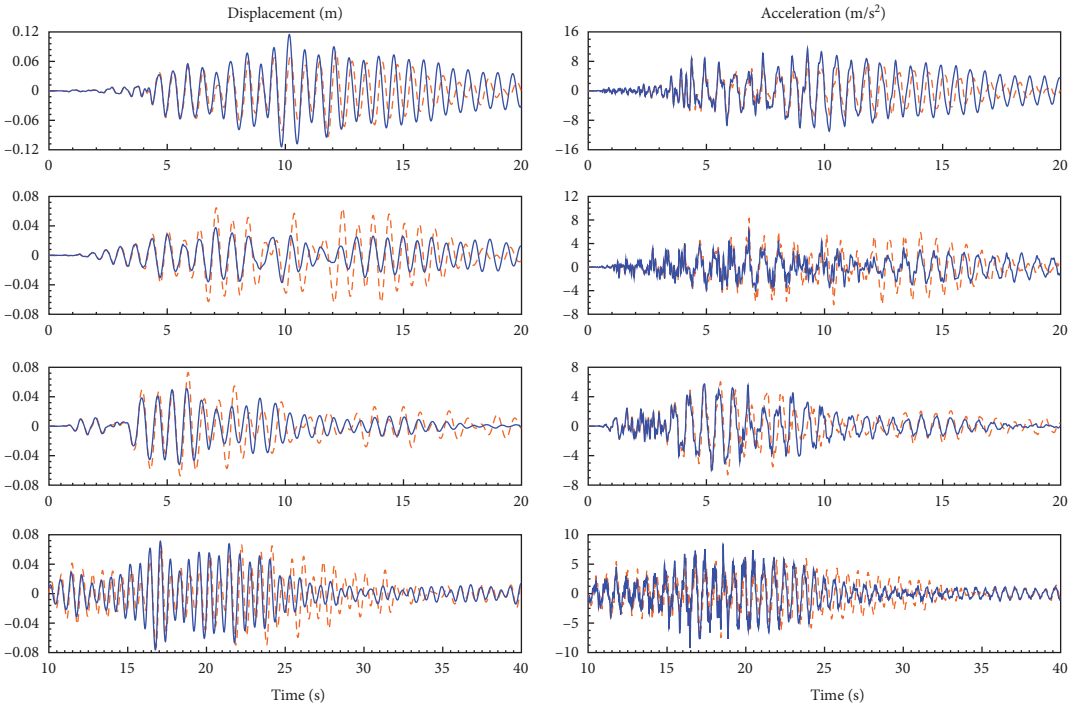

(d)

FIGURE 9: Comparison of acceleration and displacement responses at the mid-span of the longer span: (a) responses at point A; (b) responses at point B1; (c) responses at point B2; (d) responses at point D.

a reduction in the vertical displacement at point D. These findings suggest that the control of lower-order modes provided by the longer span produces a more comprehensive effect, encompassing the entire bridge. In contrast, a TMD intended for higher-order modes associated with the shorter span is less effective in mitigating the responses of the longer span.

Both schemes no. 2 and no. 3 are designed to target mode 2, but they differ in their implementation. Scheme no. 2 utilizes a concentrated mass, while scheme no. 3 utilizes a

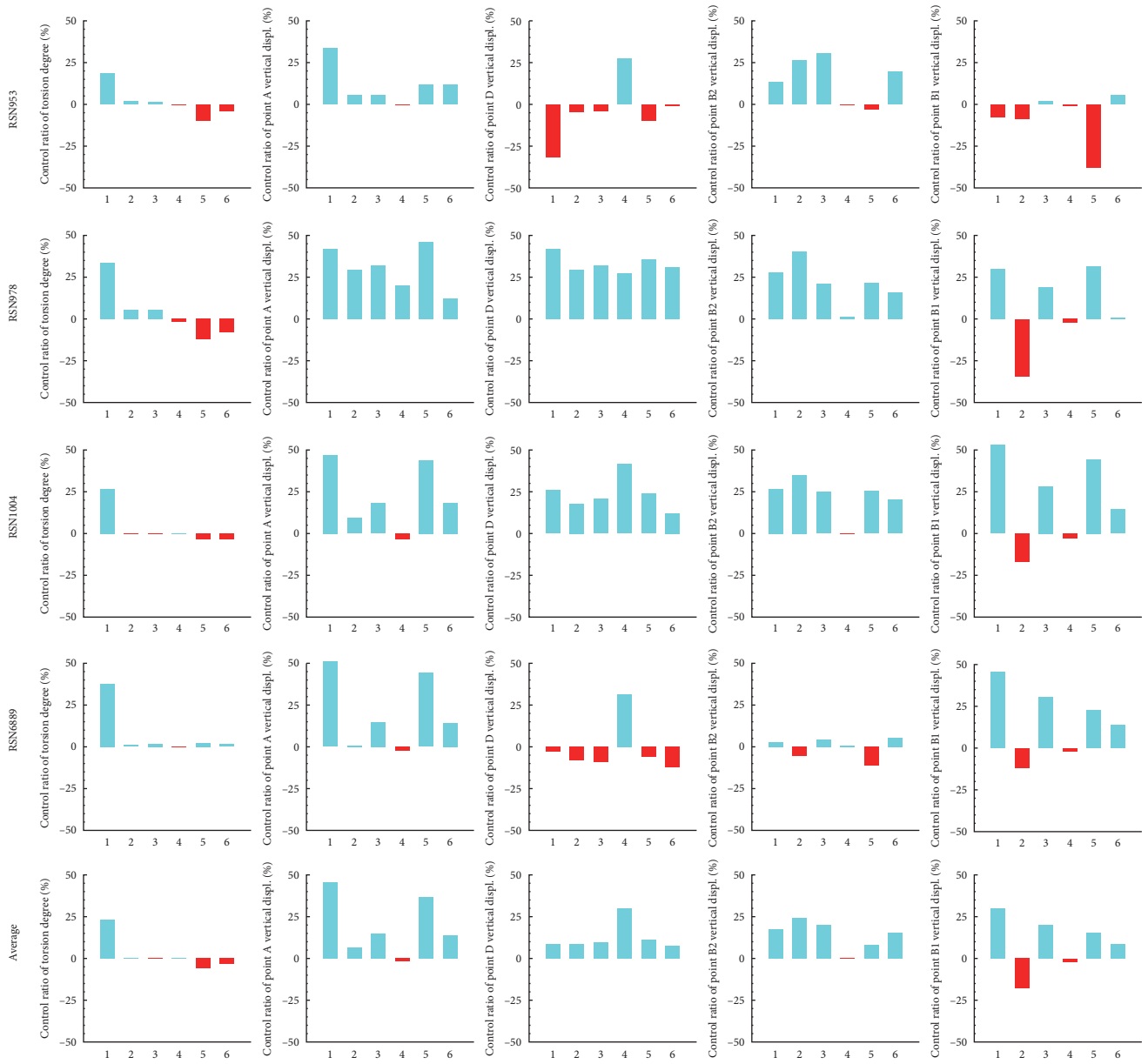

Figure 10: The control ratio of various TMD schemes for the displacements of the bridge.

distributed mass. When implemented with a concentrated mass, scheme no. 2 leads to a reduction at the TMD location but causes an increase at point B1. On the other hand, scheme no. 3, which employs symmetrically distributed masses, demonstrates better control performance, resulting in a reduction along the entire span, particularly an average reduction of about 20% at points B1 and B2. These results indicate that a TMD with distributed mass may outperform a TMD with a concentrated mass. When targeting a vibrational mode with multiple peaks, it is crucial to simultaneously consider these peak locations as potential sites for placing TMDs.

Schemes no. 3, no. 5, and no. 6 can be compared as they incorporate either a single TMD or a multimodal TMD. All of these schemes are capable of generating reductions along the entire longer span, with minimal variation in the reduction ratio across different locations. However, a notable finding is that a single TMD proves to be the most effective for the target mode. For instance, scheme no. 5 demonstrates superior effectiveness in controlling the vertical displacement at point A by a reduction ratio of 36%, while scheme no. 3 performs best at points B1 and B2, with an average reduction ratio of 20%. On the other hand, the use of a multimodal TMD results in a moderate response reduction across all locations.

Aside from displacement, member forces play a vital role as critical indicators in seismic design. To comprehensively illustrate the effects of TMD schemes, Figure 11 compares the maximum forces acting on various structural members, including the tension force of the stress ribbons, the axial force of the pier, and in-plane (bending axis: x-direction) and out-of-plane (bending axis: y-direction) bending moments at

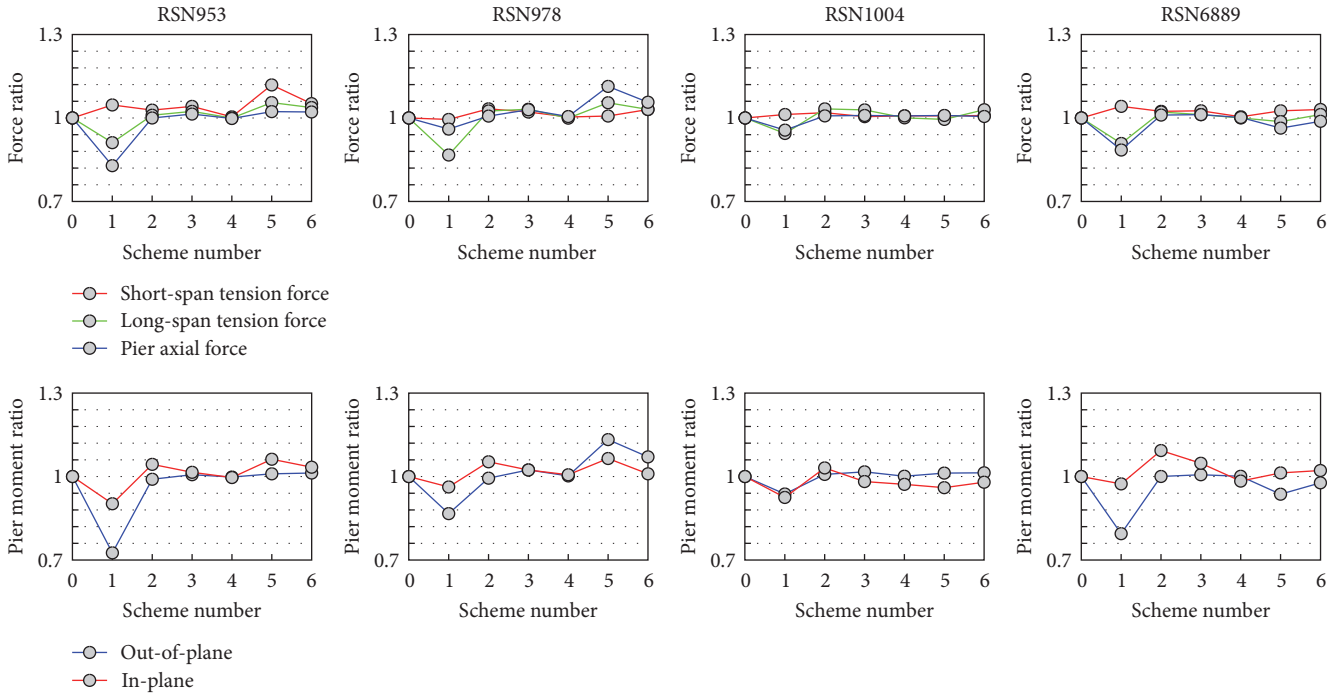

Figure 11: The ratios of member forces of the bridge models with and without TMD.

the pier base. The horizontal axis represents the scheme numbers, with "0" denoting the scenario without a TMD. From the observation, it is clear that the variation in structural member forces after the incorporation of a TMD is not as significant as the displacements. In comparison to the case without a TMD, all schemes, except for no. 1, result in an increase of up to 10% in the member forces. By comparing scheme no. 1 and no. 5, it is found that a torsional TMD can effectively reduce the pier forces, which also implies that the pier force is significantly related with the torsion response of the stress ribbons.

In addition to the factors mentioned earlier, the stroke of the TMD is another crucial consideration when selecting TMDs. A larger stroke requirement necessitates a larger space to accommodate the TMD. To illustrate this, Figure 12 showcases the hysteretic curves of TMDs for bending modes in various schemes under the excitation of the RSN956 record. In scheme no. 1 and no. 5, the vertical TMD at point A exhibits a similar displacement of approximately 0.09 m. On the other hand, scheme no. 6 demonstrates a significantly smaller amplitude of 0.025 m. Comparing schemes no. 2 and no. 3, it can be observed that distributed TMDs require a larger stroke compared to the concentrated mass. The amplitude for scheme no. 2 is approximately 0.07 m, while for scheme no. 3, it is approximately 0.055 m.

Upon careful analysis, it appears that a single TMD positioned at the center of the longer span can effectively control the displacement of the entire span. This placement offers the advantage of a straightforward installation process and meets acceptable stroke requirements. Therefore, for optimal displacement control, we recommend a scheme that includes this single TMD. Furthermore, in order to address pier forces, we suggest the addition of a torsional TMD. This additional TMD will enhance the mitigation of pier forces and further improve the overall performance of the bridge under seismic events. Taking these factors into consideration, we recommend implementing scheme no. 1, which includes a single TMD for displacement control and an additional torsional TMD for addressing torsion and pier forces.

4.3. Comparison of Responses from Different Input Orientations. The current approach to earthquake response analysis involves arbitrarily inputting two horizontal ground motions to structures without considering the direction of the input. However, studies have indicated that this method may underestimate seismic fragility, particularly in bridges [42, 43]. It has been shown that the horizontal component of earthquake excitation significantly affects the torsional response of stress-ribbon bridges. To explore the effect of input direction, an earthquake record (RSN978) was input again into the bridge with varying input angles of the horizontal components, and the impact of the vertical component was also investigated. The analysis considered four settings: (a) controlled structure with tri-directional input, (b) controlled structure with bi-directional input, (c) uncontrolled structure with tri-directional input, and (d) uncontrolled structure with bi-directional input. The input angle was varied from 0° to 90°, with an increment of 10°, where 0° denotes that the stronger horizontal component (with larger PGA) is inputted to the X-direction, and the weak component is inputted to the Y-direction, while 90° signifies a perpendicular input angle to that of 0°.

Figure 13 illustrates the displacement responses, including the vertical displacement at A, B1, and C2, and the torsional angle at A. The black and gray symbols represent the responses of the uncontrolled bridge and controlled bridge

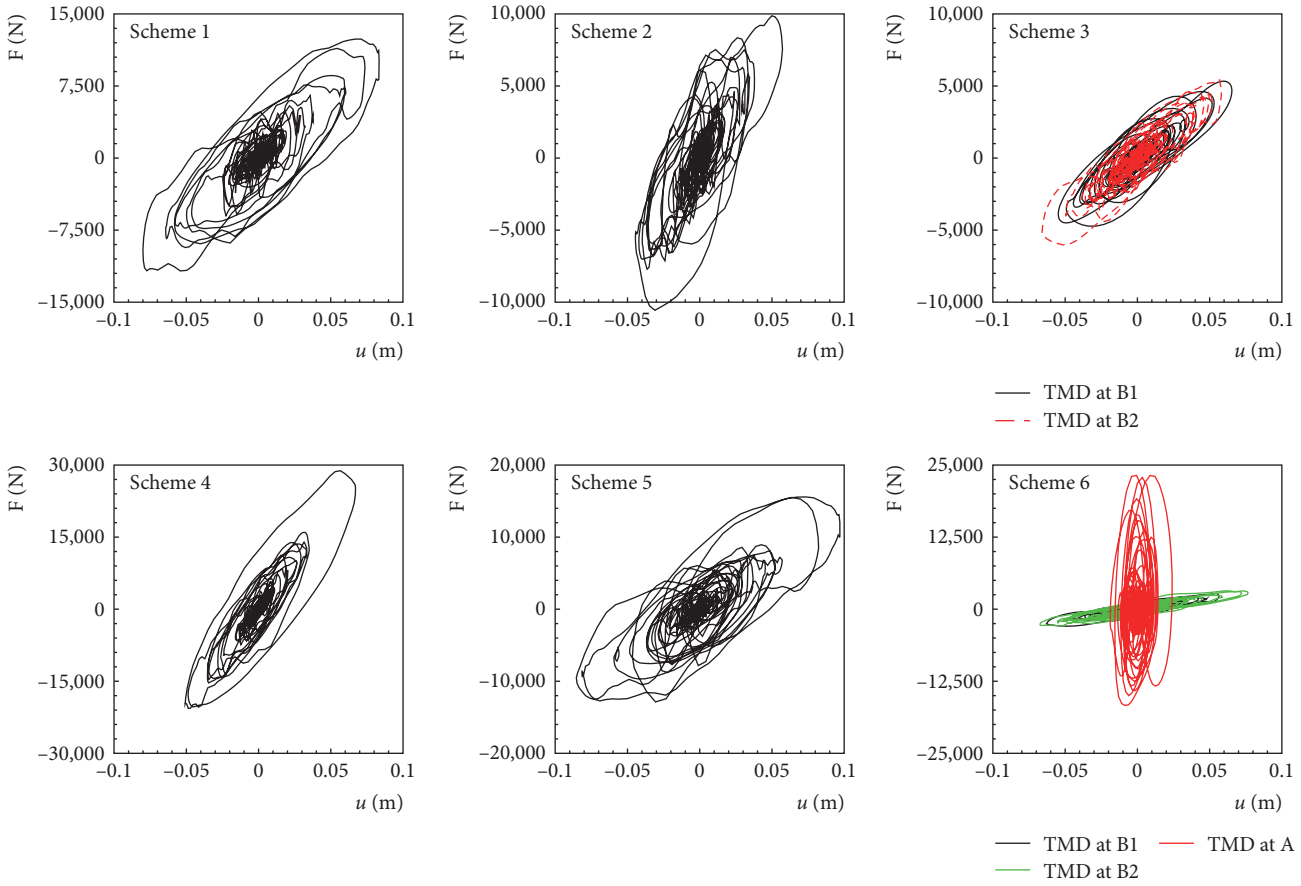

Figure 12: The hysteretic curves of TMDs of different schemes.

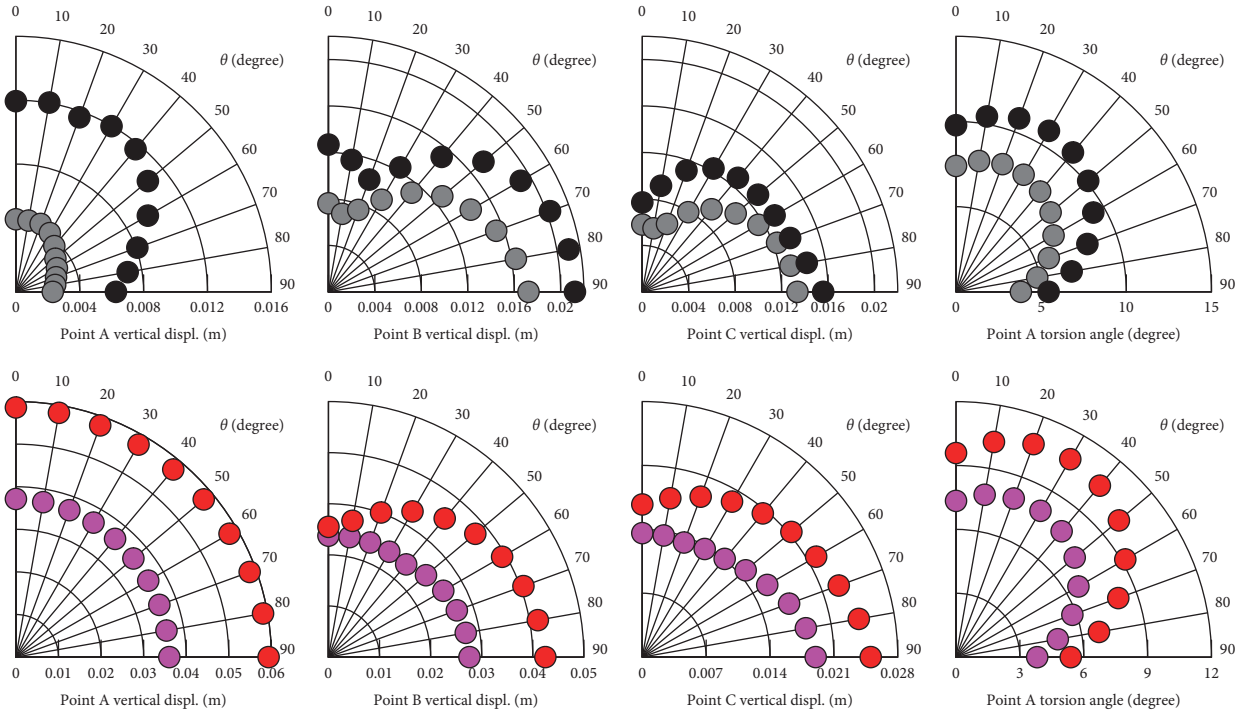

Figure 13: Displacement response resulting from different input angles.

under bi-directional horizontal excitations, respectively, while the red and purple symbols represent the forces obtained from tri-directional excitations. The vertical displacements at A, B1, and C2 are significantly increased by the vertical component of the earthquake record, emphasizing its crucial role in estimating the vertical displacement of the bridge. Regarding the torsional response, the maximum response is more than twice the minimum response resulting from different input directions. These results underscore the significance of considering the earthquake input direction in structural analysis. Responses derived from an arbitrary input direction may not accurately reflect the critical response experienced by the structure due to earthquake excitations. Additionally, the displacement can be effectively reduced by adding a TMD, and the disparity in responses arising from different input directions is also minimized.

5. Conclusions

To provide structural designers with a better understanding of the dynamic performance of stress-ribbon bridges under earthquakes, this study conducted a finite element analysis to examine the earthquake response of a steel-plated stress-ribbon bridge controlled by TMDs. The study evaluated six configuration schemes with equal mass of vertical TMDs. The following conclusions were drawn:

(1) The stress-ribbon bridge exhibits multiple vibrational modes closely spaced in frequency. The addition of TMDs to the bridge introduces both static mass and tuning effects on the modal frequency. When a TMD with a mass ratio of 0.1 is added, the fundamental frequency decreases by 12% due to the static mass effect and by 27% when considering the tuning effect as well.

(2) TMDs aimed at controlling the vertical displacement are effective in reducing vertical displacement but less effective in reducing torsional response and member forces. On the other hand, torsional TMDs can effectively reduce both torsional response and member forces simultaneously.

(3) Increasing the mass of the TMD always leads to a larger reduction in the earthquake response. The tuning effect is most significant when the mass ratio falls between 2% and 4%. Installing a single TMD for mode 1 with a mass ratio of 0.05 can decrease vertical displacement along the entire span by up to 36%.

(4) For mode 2, which has an asymmetric shape, a TMD with distributed mass outperforms one with concentrated mass.

(5) Based on the displacement and force control requirements, it is recommended to use a combination of a single TMD for mode 1 and a torsional TMD for mode 3 for earthquake response control.

(6) The vertical displacement and torsional response of stress-ribbon bridges are sensitive to vertical and transverse excitation, respectively. The orientation of earthquake excitation can significantly influence the bridge's response. However, after adding TMDs, the response dispersion resulting from the input orientation is reduced.

Data Availability

The data used to support the findings of this study are available from the corresponding author upon request.

Conflicts of Interest

The authors declare there are no conflicts of interest regarding the publication of this paper.

Acknowledgments

The PEER strong motions database is greatly acknowledged for providing valuable ground motion data.

References

[1] A. Goldack, M. Schlaich, and M. Meiselbach, "Stress ribbon bridges: mechanics of the stress ribbon on the saddle," *Journal of Bridge Engineering*, vol. 21, no. 5, Article ID 04015089, 2016.

[2] A. Juozapaitis, G. Sandovič, R. Jakubovskis, and V. Gribniak, "Effects of flexural stiffness on deformation behaviour of steel and FRP stress-ribbon bridges," *Applied Science*, vol. 11, no. 6, Article ID 2585, 2021.

[3] A. Bleicher, M. Schlaich, Y. Fujino, and T. Schauer, "Model-based design and experimental validation of active vibration control for a stress ribbon bridge using pneumatic muscle actuators," *Engineering Structures*, vol. 33, no. 8, pp. 2237–2247, 2011.

[4] C. Moutinho, A. Cunha, and E. Caetano, "Analysis and control of vibrations in a stress-ribbon footbridge," *Structural Control and Health Monitoring*, vol. 18, no. 6, pp. 619–634, 2011.

[5] J. M. Soria, I. M. Díaz, E. Pereira, J. H. García-Palacios, and X. Wang, "Exploring vibration control strategies for a footbridge with time-varying modal parameters," *Journal of Physics: Conference Series*, vol. 744, Article ID 012170, 2016.

[6] W.-H. Hu, E. Caetano, and Á. Cunha, "Structural health monitoring of a stress-ribbon footbridge," *Engineering Structures*, vol. 57, pp. 578–593, 2013.

[7] J. M. Soria, I. M. Díaz, J. H. García-Palacios, and N. Ibán, "Vibration monitoring of a steel-plated stress-ribbon footbridge: uncertainties in the modal estimation," *Journal of Bridge Engineering*, vol. 21, no. 8, Article ID C5015002, 2016.

[8] C. Moutinho, Á Cunha, E. Caetano, and J. M. de Carvalho, "Vibration control of a slender footbridge using passive and semiactive tuned mass dampers," *Structural Control and Health Monitoring*, vol. 25, no. 9, Article ID e2208, 2018.

[9] X. Xiao, Y. Chen, W. Shen, and H. Zhu, "Vibration control of stress ribbon bridges subjected to moving vehicles," *Structural Control and Health Monitoring*, vol. 28, no. 12, Article ID e2835, 2021.

[10] T. Igusa and K. Xu, "Vibration reduction characteristics of distributed tuned mass dampers," in *Proceedings of the Fourth International Conference on Recent Advances in Structural Dynamics*, M. Petyt, Ed., pp. 596–605, Southampton, USA, 1991.

[11] E. Caetano, Á. Cunha, C. Moutinho, and F. Magalhães, "Studies for controlling human-induced vibration of the Pedro e Inês footbridge, Portugal. Part 2: Implementation of tuned mass dampers," *Engineering Structures*, vol. 32, no. 4, pp. 1082–1091, 2010.

[12] X. Luo, R. Ma, G. Li, and D. Zhao, "Parameter optimization of multi-mode vibration control system," in *International Conference of Measuring Technology and Mechatronics Automation*, pp. 685–688, IEEE Computer Society, Piscataway, NJ, 2009.

[13] G. Chen and J. Wu, "Optimal placement of multiple tune mass dampers for seismic structures," *Journal of Structural Engineering*, vol. 127, no. 9, pp. 1054–1062, 2001.

[14] Y. Daniel, O. Lavan, and R. Levy, "Multiple-tuned mass dampers for multimodal control of pedestrian bridges," *Journal of Structural Engineering*, vol. 138, no. 9, pp. 1173–1178, 2012.

[15] N. Debnath, A. Dutta, and S. K. Deb, "Multi-modal passive-vibration control of bridges under general loading-condition," *Procedia Engineering*, vol. 144, pp. 264–273, 2016.

[16] K. Xu, Q. Dai, K. M. Bi, G. S. Fang, and L. Zhao, "Multi-mode vortex-induced vibration control of long-span bridges by using distributed tuned mass damper inerters (DTMDIs)," *Journal of Wind Engineering and Industrial Aerodynamics*, vol. 224, no. 2022, Article ID 104970, 2022.

[17] L. Romera, S. Hernandez, A. Baldomir, and F. Nieto, "Study of pedestrian comfort in a three span stress ribbon footbridge with carbon fibre cables," *WIT Transactions on the Built Environment*, vol. 196, pp. 139–151, 2020.

[18] Y. Kajikawa, S. Fukada, and H. Yoshikawa, "Vibration characteristics of prestressed concrete stress ribbon," in *Proceedings of Colloquium on Bridge Vibration*, p. 175, (in Japanese), 1997.

[19] Y. Kajikawa, Y. Touge, S. Fukada, and K. Matsumoto, "Vibration test and analysis on 4-span continuous stress-ribbon bridge with a roadway slab," *Journal of Structural Engineering*, vol. 44A, (in Japanese), Article ID 835, 1998.

[20] Y. Kajikawa, S. Fukada, and T. Kuribayashi, "Vibration serviceability and characteristics of branching three ways stress ribbon pedestrian," *Journal of Structural Engineering*, vol. 45A, (in Japanese), Article ID 633, 1999.

[21] Y. Touge, S. Fukada, and Y. Kajikawa, "Vibration characteristics of prestressed concrete stress ribbon bridge with a roadway slab deck due to traffic," in *Proceedings of Colloquium on Bridge Vibration*, p. 147, (in Japanese), 1997.

[22] T. Aso, K. Uno, Y. Fujimoto, H. Okazaki, and M. Watanabe, "Dynamic characteristics and earthquake response analysis of three-span continuous stress ribbon bridge," 12WCEE, 2000.

[23] I. G. Buckle, *The Northridge, California Earthquake of January 17, 1994: Performance of Highway Bridges*, National Center for Earthquake Engineering Research, American Society Civil Engineers, Buffalo, NY, 1994.

[24] M. C. Gómez Soberón and J. M. Gómez Soberón, "Dynamic properties variation by irregular superstructure and substructure common bridges," *Procedia Engineering*, vol. 199, pp. 2961–2966, 2017.

[25] K. Kawashima, S. Unjoh, J.-I. Hoshikuma, and K. Kosa, "Damage of bridges due to the 2010 Maule, Chile, earthquake," *Journal of Earthquake Engineering*, vol. 15, no. 7, pp. 1036–1068, 2011.

[26] R. Akbari and S. Maalek, "A review on the seismic behaviour of irregular bridges," *Proceedings of the Institution of Civil Engineers —Structures and Buildings*, vol. 171, no. 7, pp. 552–580, 2018.

[27] D. G. Smith, "Field assessment of unforeseen earthquake induced bridge deck movements & probable effects of geometry," in *Proceedings of the 4th European Workshop on the Seismic Behaviour of Irregular and Complex Structures*, pp. 26-27, 2005.

[28] A. S. Elnashai, B. Gencturk, O. S. Kwon et al., "The Maule (Chile) earthquake of February 27, 2010: consequence assessment and case studies," Mid-America Earthquake Center Report No. 10-04, 2010.

[29] C. M. Casado, I. M. Díaz, J. D. Sebastian, A. V. Poncela, and A. Lorenzana, "Implementation of passive and active vibration control on an in-service footbridge," *Structural Control and Health Monitoring*, vol. 20, no. 1, pp. 70–87, 2013.

[30] E. Bayat, M. Bayat, and R. Hafezzadeh, "Numerical performance assessment of tuned mass dampers to mitigate traffic-induced vibrations of a steel box-girder bridge," *Structural Engineering and Mechanics*, vol. 78, no. 2, pp. 125–134, 2021.

[31] X. W. Huang, J. Zhao, Z. Zheng, and Y. L. Song, "Parameter calibration and application of GTN model of Q690D high strength steel," *Industrial Construction*, vol. 48, no. 8, pp. 163–168, (In Chinese), 2018.

[32] S. Chen, Z. Lu, G. Li, M. Wei, Y.-B. Wang, and X. Chen, "Cyclic loading tests of Q690D high strength steel welded columns," *Journal of Building Structures*, vol. 35, no. 12, pp. 97–103, (In Chinese), 2014.

[33] J. Strasky, *Stress-Ribbon and Supported Cable Pedestrian Bridges*, Thomas Telford Ltd, London, 2nd edition, 2011.

[34] G. Sandovic, A. Juozapaitis, and V. Gribniak, "Experimental and analytical investigation of deformations and stress distribution in steel bands of a two-span stress-ribbon pedestrian bridge," *Mathematical Problems in Engineering*, vol. 2017, Article ID 9324520, 11 pages, 2017.

[35] S. Hiejima and Y. Fujino, "Approximate solutions for natural frequencies and modes of stress ribbon bridge," *Journal of Structural Engineering*, vol. 39A, (in Japanese), Article ID 819, 1993.

[36] J. Radnic, D. Matesan, and D. Buklijas-Kobejevic, "Numerical model for analysis of stress-ribbon bridges," *Gradevinar*, vol. 67, pp. 959–973, 2015.

[37] Y. Zhang, W. C. Pu, Q. S. Zhang, K. W. Liu, and H. Dong, "Effect of ground motion orientation on seismic responses of an asymmetric stress ribbon pedestrian bridge," *Advances in Civil Engineering*, vol. 2022, Article ID 1278314, 12 pages, 2022.

[38] D. C. del Arco, Á.C. Aparicio, and A. R. Mafı, "Preliminary design of prestressed concrete stress ribbon bridge," *Journal of Bridge Engineering*, vol. 6, no. 4, pp. 234–242, 2001.

[39] M. Cacho-Perez, N. Frechilla, I. Diaz, and A. Lorenzana, "Simplified mechanical model for a stress-ribbon monitorized footbridge: analytical and experimental results," in *Proceedings, 6th World Conference on Structural Control and Monitoring, International Center for Numerical Methods in Engineering*, pp. 358–368, Barcelona, Spain, 2014.

[40] R. Rana and T. T. Soong, "Parametric study and simplified design of tuned mass dampers," *Engineering Structures*, vol. 20, no. 3, pp. 193–204, 1998.

[41] PEER, "Pacific earthquake engineering research center: strong motion database," 2013, http://peer.berkeley.edu/smcat.

[42] M. Torbol and M. Shinozuka, "Effect of the angle of seismic incidence on the fragility curves of bridges," *Earthquake Engineering & Structural Dynamics*, vol. 41, no. 14, pp. 2111–2124, 2012.

[43] S. B. Basu and M. Shinozuka, "Effect of ground motion directionality on fragility characteristics of a highway bridge," *Advances in Civil Engineering*, vol. 536171, Article ID 536171, 12 pages, 2011.